High-Throughput Single Particle Characterization of Aggregation Pathways and the Effects of Inhibitors for Large (Megadalton) Protein Oligomers

For submission to: *Analytical Chemistry*

Jacob S. Jordan, Conner C. Harper, and Evan R. Williams*

Department of Chemistry, University of California, Berkeley, California, 94720-1460

*To whom correspondence should be addressed

e-mail: erw@berkeley.edu

Abstract

Protein aggregation is involved in many human diseases, but characterizing the sizes and shapes of intermediate oligomers (~10 – 100 nm) important to the formation of macroscale aggregates like amyloid fibrils is a significant analytical challenge. Here, charge detection mass spectrometry (CDMS) is used to characterize individual conformational states of bovine serum albumin oligomers with up to ~225 molecules (15 MDa). Elongated, partially folded, and globular conformational families for each oligomer can be readily distinguished based on the extent of charging. The abundances of individual conformers vary with changes in the monomer concentration or by adding aggregation inhibitors, such as SDS, heparin, or $MgCl_2$. These results show the potential of CDMS for investigating intermediate oligomers in protein aggregation processes that are important for understanding aggregate formation and inhibition mechanisms and could accelerate formulation buffer development to prevent the aggregation of biotherapeutics.

Introduction

Protein aggregation is involved in many human diseases including Alzheimer's, Parkinsons', and Huntingtons' disease, dementia, amyotrophic lateral sclerosis (ALS), type-2 diabetes, and transmissible spongiform encephalopathies.[1] Understanding aggregation mechanisms and pathways is important for developing effective drugs and treatments for inhibiting the progression of disease. Protein-based therapeutics also aggregate under a wide range of stress conditions which can cause inefficacy and toxicity *in vivo*.[2] Developing buffer systems to prevent aggregate formation for the effective transport and storage of biotherapeutics is a critical part of any drug development workflow and requires the characterization of aggregates formed after stress in many different solution conditions.

Small proteinaceous oligomers can be characterized by many different methods, including size-exclusion chromatography,[3] mass photometry,[4–8] and mass spectrometry.[9] Information about the average size of much larger complexes formed after extensive aggregation occurs can be obtained from light scattering methods.[10] A variety of different microscopy techniques can provide individual particle data from which distributions of particle size and shape can be determined.[11] However, little is known about intermediate size aggregates that have masses in the MDa range. This is due in part to molecular complexity and the short-lived nature of what can be transient species that are challenging to measure using existing methods.

Native mass spectrometry has significant advantages for characterizing smaller oligomeric states of proteins. In combination with ion mobility spectrometry (IMS), information about the abundances and shapes of individual oligomers has been obtained for different proteins and peptides implicated as precursors in human disease, including Aβ42,[12–15] Tau,[16–18] TDP-43,[19,20] and α-synuclein.[21–23] Information about the secondary structure elements of aggregate forming

peptide oligomers has been obtained through the combination of gas-phase infrared spectroscopy with IMS-MS.[24–26] However, characterizing full length proteins or higher order aggregates using these techniques is hampered by the mass range of conventional MS instruments that measure ensembles of ions. Although general structural information can be inferred based on the extent of protein charging,[27,28] complex mixtures of high molecular mass species can lead to charge-state distributions with overlapping *m/z* values that obscure information about ion charge and hence mass and shape from being obtained.[29]

Charge detection mass spectrometry, in which the *m/z* and charge of individual analyte ions are measured simultaneously, overcomes the mass and charge limitations of conventional MS instruments. CDMS instruments have been used to investigate large protein complexes[30–32] and molecular machines,[33,34] intact viruses[35–38] and virus-like particles,[39,40] salt clusters,[41] and synthetic polymers,[42,43] as well as aqueous nanodroplets[44,45] and nanoparticles with masses that extend into the GDa range.[46,47] By distinguishing individual species across a wide range of masses and shapes, CDMS can provide a better overview of sample composition than more conventional methods such as transmission electron microscopy, dynamic light scattering, size-exclusion chromatography, or analytical ultracentrifugation.[46–48] The high mass capabilities of CDMS are well suited to measuring a broad mass range of oligomers formed by aggregation in solution.[48–50] Here, aggregates of the model protein bovine serum albumin (BSA) are formed during heat stress under a variety of solution conditions. CDMS measurements of these complex mixtures with and without aggregation inhibitors demonstrate the advantages of CDMS for characterizing the sizes and conformations of protein oligomers in a mass range that has not been previously accessible using conventional analysis methods.

Experimental

Thermal Stress Protocol. Aqueous solutions of 0.1 – 37 mg/mL (~1.5 – 550 μM) bovine serum albumin (BSA) with 50 mM ammonium acetate (pH 6.8) were heated to 75 ˚C for 20 minutes using a dry bath incubator (Fisher Scientific, Hampton, NH). Optical density measurements were taken immediately after heat-stress without filtering the solution using a ThermoFisher Nanodrop One UV-Vis Spectrophotometer (Thermofisher Scientific, Waltham, MA). For mass spectrometry analysis, samples were vortexed and filtered through a 0.22 μm syringe filter (Thermofisher Scientific) to remove insoluble aggregates. For inhibition experiments, sodium dodecyl sulfate (SDS) and heparin (5 kDa average molecular weight) were added in molar equivalent ratios of 1:4 and 1:1 to 5 mg/mL aqueous BSA solutions containing 50 mM ammonium acetate. 5 mg/mL BSA in 50 mM ammonium acetate and 200 mM $MgCl_2$ were used to test the inhibitory effect of $MgCl_2$. BSA, $MgCl_2$, and ammonium acetate were obtained from Sigma-Aldrich (St. Louis, MO). Heparin and SDS were obtained from Fisher Scientific (Pittsburgh, PA). All reagents were used without further purification.

Charge Detection Mass Spectrometry. Ions were formed by electrospray ionization from borosilicate nanoelectrospray emitters fabricated in-house from borosilicate capillaries (0.78 mm inner diameter, 1.00 mm outer diameter, Sutter Instrument, Novato, CA) pulled to a final inner diameter of 1.3 ± 0.1 μm using a Sutter Instrument P-87 Flaming/Brown micropipette puller.[51] Emitter tip diameters were imaged using a Hitachi TM-1000 microscope (Tokyo, Japan) at the University of California, Berkeley - Electron Microscopy Laboratory. Charge detection

mass spectrometry experiments were performed using a custom-built instrument. Both this instrument and the data analysis methods are described in detail elsewhere.[46,47,52,53] This instrument consists of a heated ion transfer tube (140 °C), three RF-only quadrupole ion guides, and an electrostatic cone trap. Ion transmission over a wide range of *m/z* values was achieved by varying the RF voltages and frequencies applied to the quadrupoles and ion funnel.

Results and Discussion

Soluble Protein Oligomer Size and Conformation. Bovine serum albumin (BSA) can form both fibrillar and amorphous aggregates within minutes at temperatures higher than ~60 °C. The performance of CDMS for characterizing protein oligomers in the MDa size range was evaluated by measuring mass and charge data from solutions containing 5 mg/mL (~75 μM) bovine serum albumin (BSA) before and after heating at 75 °C for 20 minutes. A CDMS mass histogram (Figure 1a) obtained from an unheated solution shows resolved oligomers up to hexamers (~405 kDa) and unresolved oligomers with masses between 0.5 – 2.5 MDa (7 – 37 molecules). The low signal for oligomers with masses between 300 kDa and 500 kDa, as well as the observation that the higher mass aggregates disappear upon addition of a small molecule (see below), indicate that these aggregates exist in solution and are not an artifact of the electrospray process. QTOF mass spectra of this solution shows low-charge forms of abundant monomer up to a low abundance hexamer, corresponding to compact, folded structures in solution (Figure S1). The baseline at *m/z* >10,000 is slightly elevated, and this is likely due to larger, unresolved globular aggregates that are clearly detected by CDMS. After heating the solution at 75 °C for 20 minutes, individual BSA oligomers up to the 23-mer are well-resolved by CDMS (Figure 1b) and

there is unresolved signal up to ~15 MDa (~225 molecules) (Figure S2). There are single ions that appear between ~15 – 20 MDa. The detection threshold was set at ~15 charges for this CDMS analysis, and counts in this mass range correspond to individual ions with more than 100 charges. Therefore, even these single counts at these high masses and charges correspond to real, high molecular weight ions. The appearance of these oligomers from the heated sample, but not from the unheated sample, indicates that these aggregates were formed due to solution heating. The lower resolution obtained for the larger aggregates without heating is likely due to adducting salts and small molecules that can be dissociated from the protein when a solution is heated.[54]

An advantage of CDMS analysis is that because both the mass and charge of an ion are measured simultaneously, data can be plotted as a two-dimension histogram. A 2D histogram for the heated sample of BSA in Figure 1b shows four distinct conformer families, indicated by the different colored regions in Figure 2a, that extend over a wide range of both mass and charge. These conformer families, denoted as I, II, III, and IV, are distinguished based on different extents of charging for ions that have the same mass. The blue dashed line in Figure 2a is the calculated Rayleigh charge limit for a spherical water nanodrop with a given mass and charge. In native mass spectrometry, proteins and protein complexes typically charge to ~80% of the Rayleigh limit, consistent with compact forms associated with native structures.[55] In contrast, highly elongated ions charge significantly above the Rayleigh limit. Oligomers in conformer family **I**, indicated by the green shaded region, are charged close to the Rayleigh limit (Figure 2a). A mass histogram of just this green region (Figure 2b) shows a monomer and oligomers as large as the 14-mer (~1 MDa). Conformer family **II** contains aggregates charged well below the Rayleigh limit (Figure 2a, purple region) that span from 1.0 MDa (~15 molecules) up to ~15

MDa (~225 molecules) in size (Figure 2c). The lower charge compared to the Rayleigh limit is consistent with more compact globular structures. The maximum oligomer size of conformer family **I** overlaps in mass with the minimum oligomer size of conformer family **II**, indicating that conformer family **I** may convert into conformer family **II** in this overlapping oligomer size range.

Conformer family **III** (Figure 2a, blue region) consists of highly charged oligomers that start at the trimer and are well-resolved to the 24-mer, although ion signals up to ~2 MDa (~30 BSA molecules, Figure 2d) are observed. These conformers are charged well above the Rayleigh limit and show a near linear increase in charge with increasing mass, indicating that these structures must be elongated in solution. Conformer family **IV** (Figure 2a, orange region) has charge states between those of the highly extended (**III**) and compact forms (**I** and **II**) of BSA oligomers. The range of charge states is broader than it is for the other conformer families indicating that this family of structures can take on a range of conformations between those of the compact and highly extended forms. A BSA dimer formed from a solution of water/methanol/acetic acid in which BSA is denatured has charge states between +37 and +93 (Figure S3). In contrast, the BSA trimer in family **III** has charge states between ~+30 and +49 (Figure 2a). This indicates that although the trimer and higher order structures of family **III** and **IV** are extended, they are not as extended as fully denatured dimers. This suggests a structure in which more folded monomers are forming extended structures.

The abundance of small oligomers (<5 BSA molecules) charged above the Rayleigh limit in unheated solutions is very low (Figure S4), indicating that the vast majority of the two extended conformer families are formed in solution after heating (Figure 2a) and are not an artifact of the electrospray ionization process. No highly charged BSA monomers are observed

after heat stress, indicating that the high-charge ions of conformer family **III** do not originate from gas-phase collision-induced dissociation of even larger oligomers. Individual conformers are mass resolved up to ~1 MDa (~15 BSA molecules). Oligomers above this mass are not individually resolved, likely due to salt or other small molecule adducts that broaden peaks. The BSA monomer and dimer have compact structures and there are no higher charged forms present. This indicates that unfolding of both of these species at 75 ˚C is reversible. In contrast, the extended structures of the unfolded trimer and higher order aggregates indicate that their formation is irreversible and produces long-lived aggregates that are stable at room temperature. Thus, it appears that the extended trimer is critical to the formation of larger aggregates that have highly elongated structures.

These data demonstrate the advantage of CDMS to resolve distinct conformation families of individual protein oligomers formed during heat stress based on the ability to measure both mass and charge. The oligomers readily resolved in the 2D mass-charge histogram in Figure 2a are completely unresolved in *m/z* space (Figure S5), highlighting the advantage of the simultaneous measurements of mass and charge of individual ions for samples containing highly heterogenous analytes that overlap significantly in *m/z*.

Aggregation Pathways Depend on Initial Monomer Concentration. Protein aggregation and the types of structures (amorphous, fibrils, etc.) generated upon stress depend on concentration. To investigate how the initial monomer concentration affects the abundance of the conformational families identified in Figure 2a, solutions containing 0.1 – 37 mg/mL (~1.5 – 550 μM) BSA were heat-stressed for 20 min at 75 ˚C and the resulting aggregation products characterized using CDMS. From unheated solutions containing 0.1 mg/mL BSA, there are

compact oligomers up to the hexamer with little higher order aggregates (Figure S6a). After heating, there is abundant monomer and dimer as well as compact aggregates of conformer family **II** with masses up to 2.0 MDa (30 molecules) (Figure S6b). The absence of solution turbidity and a low OD_{600} after heating indicate that these aggregates are sufficiently small to remain soluble (Figure S7, Figure S8).

At concentrations $\geq$1 mg/mL, there are both elongated and compact higher-order oligomers after heat stress (Figure 3). At 1 mg/mL, oligomers in compact conformer family **I** extend past 30-mers (2 MDa) and overlap in size with conformer family **II**, which extends from ~22-mers (~1.5 MDa) to 119-mers (~8 MDa) (Figure 3a). At 5 – 15 mg/mL, the average molecular mass of conformer family **I** is reduced with increasing concentration (Figure 3a-c). whereas both the average molecular mass and the abundances of conformer family **II** increase between 1 - 5 mg/mL before decreasing at higher concentrations. The abundance of conformers **III** and **IV** is higher at 5 and 10 mg/mL compared to 1 mg/mL. Above 10 mg/mL, the abundance of conformer families **I**, **II**, and **III** is reduced (Figure S9). This is likely due to the rapid formation of larger, insoluble aggregates that are filtered out prior to the CDMS measurement (Figure S6). The OD_{600} of samples with BSA concentrations >10 mg/mL increases linearly with increasing concentration up to 37 mg/mL, indicating a higher turbidity than lower concentration samples (Figure S8). These data are consistent with the formation of larger aggregates with increasing protein concentration.

Increasing the initial concentration and monitoring the abundances of the conformational families provides information about how concentration affects different aggregation pathways. Decreased abundance for any family suggests the formation of higher order, insoluble aggregates

of the same family that deplete the population of small oligomers or conversion to a different conformer family. The compact families **I** and **II** decrease in abundance above 1 mg/mL and 5 mg/mL, respectively, indicating the formation of large, amorphous aggregates, consistent with a small increase in the OD_{600} (Figure S8). The increase in abundance of the elongated conformers **III** and **IV** at 5 mg/mL and subsequent decrease in abundance at concentrations above 5 mg/mL and 10 mg/mL, respectively, indicate that the formation of large, elongated aggregates occurs at a higher concentration than compact aggregates of conformer families **I** and **II**. These data are consistent with prior work on different amyloid-forming proteins, wherein forming amorphous aggregates proceeds without a lag-phase and is kinetically favored over the formation of amyloid fibrils, which require significant changes to protein secondary and tertiary structure and the formation of specific, fibril-competent structures to initiate fibrillation.[56] At concentrations >10 mg/mL where conformations **III** and **IV** are reduced in abundance, the turbidity increases and there is a significant increase in viscosity (Figure S7, S8). The increase in viscosity at concentrations where the abundance of conformer families **III** and **IV** are depleted indicates that the larger elongated/fibril-like aggregates may initiate gel formation. These results show the promise of CDMS for investigating aggregation pathways in a size range where other biophysical techniques cannot resolve individual oligomer conformations.

Aggregation Inhibitors Decrease the Formation of Specific Conformations.

Aggregation inhibitors can affect the distributions and conformations of aggregates that are formed upon heat stress. Sodium dodecyl sulfate (SDS) is known to completely inhibit BSA aggregation.[57] As a control experiment, solutions containing 5 mg/mL BSA and 4 molar eq. sodium dodecyl sulfate (SDS) detergent were heated to 75 ˚C for 20 min. Only compact

monomer, dimer and a low abundance of trimer were observed, indicating that SDS prevents formation of all higher order aggregates irrespective of their structure (Figure 4b compared to the reference solution without SDS shown in Figure 4a). This result indicates that SDS interferes with the oligomerization process by preventing the formation of the elongated trimer. The absence of conformer family **II** in these data confirms that these species exist in both unheated (Figure 1a) and heated solutions (Figure 3a) and are dissociated upon addition of SDS. There were no changes in turbidity after heating in the presence of SDS, indicating that the absence of signal for small oligomers in these data is due to inhibition of the aggregation process rather than acceleration to form higher order oligomers. These data indicate that SDS prevents the formation of elongated (fibril-like) BSA aggregates, consistent with prior transmission electron microscopy results,[57] and also indicate that formation of an elongated trimer is critical for the formation of irreversible aggregates.

The glycosaminoglycan heparin has been reported to inhibit BSA aggregation,[58,59] although this same molecule can act as an initiator of aggregation for other proteins.[60] Heating a 5 mg/mL BSA solution at 75 ˚C for 20 min with 1 molar eq. heparin (average MW ~5 kDa) resulted in the formation of compact oligomers (**I**) as large as the 10-mer and partially elongated species (**IV**) (Figure 4c). Globular aggregates (**II**) that range from 1 – 6 MDa (15 – 89 molecules) were also formed compared to up to ~15 MDa (~222 molecules) in samples without heparin. Heparin prevents the formation of elongated (highly charged) forms of each oligomer, consistent with the reported anti-amyloid behavior of this MW heparin.[61] The absence of conformer family **II** between 6 and 15 MDa with heparin (Figure S10) indicates that heparin also inhibits the self-association of compact forms of BSA, consistent with prior reports using higher molecular weight

heparins (~15 kDa) at lower pH and ionic strengths.[58] The intermediate charged oligomers (**IV**) observed in the presence of heparin may be aggregating via a different mechanism that utilizes a portion of the protein that heparin does not strongly interact with. Their lower abundance compared to the sample without heparin indicates they are destabilized in the presence of heparin, suggesting that heparin is partially inhibiting the oligomerization process along this pathway as well. These data are in agreement with prior literature that indicate that heparin effectively combats amyloid formation and provide novel information about the heparin mechanism of action: the selective inhibition of fully elongated oligomers and destabilization of partially elongated oligomers and high mass globular aggregates.

The addition of $MgCl_2$ at high ionic strength has also been reported to prevent BSA aggregate formation.[62] CDMS 2D mass-charge histograms of 5 mg/mL BSA with 200 mM $MgCl_2$ acquired after heat-stress show compact (**I**) and partially elongated (**IV**) oligomers, as well as a low abundance of elongated (**III**) oligomers (Figure 4d). Compact oligomers up to the tetramer are formed in the presence of $MgCl_2$ compared to the 11-mer without $MgCl_2$. Higher charge oligomers are more difficult to resolve in these data, likely due to extensive adduction of $MgCl_2$. There is no evidence for "magic" number clusters above 0.5 MDa, so loss of individual oligomer resolution does not adversely affect conclusions drawn from these data. These data indicate that $MgCl_2$ stabilizes oligomers with a partially elongated structure, preventing the formation of large amorphous aggregates as well as highly extended aggregates and provides additional evidence that partially elongated BSA oligomers are formed via a different mechanism than globular or fully elongated, amyloid-like conformers. Aggregate formation may be inhibited by specific interactions between the protein and Mg^{2+} or as a result of the change in ionic strength upon

addition of 200 mM $MgCl_2$. There was no increase in the hydrodynamic radius determined from light scattering data from 80 ˚C heat-stressed BSA (0.1 mg/mL) in the presence of 200 mM Mg^{2+} compared to a ~50 nm increase in the average hydrodynamic radius without Mg^{2+}, indicating that aggregation was inhibited.[62] Conformer **IV** aggregates detected after heat stress in the presence of Mg^{2+} by CDMS are low abundance and dispersed over a wide mass range and may not have been detected by the earlier ensemble dynamic light scattering measurements.

For each of these solution additives, the average charge state of the BSA monomer, dimer, trimer, and tetramer are the same, indicating that protein charging is not significantly affected by the presence of these additives and that they do not measurably affect the ESI process. This provides additional evidence that the very different abundances of each conformer family in the CDMS data for each additive are due to differences in their abundances in solution. These data indicate CDMS has significant advantages for characterizing the masses and shapes of oligomers in the hundreds of kDa to 10+ MDa size range. Results for the three inhibitors used here are in agreement with prior results from the literature and also provide novel information about three different mechanisms of action involving the selective inhibition of specific structures that can be readily distinguished by their "aggregation footprint" in mass and charge space.

Conclusions

CDMS measurements of oligomer size and conformation are enabled through simultaneous measurements of both *m*/*z* and charge for each individual ion. For BSA, information about oligomers consisting of over 200 protein molecules with masses up to 15 MDa was obtained. Four distinct conformer families of oligomers are resolved based on the extent of

charging at a given size. The abundances of these families depend on the initial protein concentration and is affected by the presence of inhibitors. SDS, heparin and $MgCl_2$ all reduce aggregation and information about which aggregation pathways are inhibited is obtained from the sizes and abundances of each resolved conformational family. The ability to monitor the kinetics of amyloid fibril or amorphous aggregate formation makes CDMS a promising technique for obtaining information at the earliest stages of the aggregation process without the need for microscopy methods that require extensive sample preparation or the need to wait until much larger aggregates that can be optically detected are formed. Further experiments comparing information obtained from different methods on standard samples would highlight the relative advantages of various techniques used to quantify protein aggregation.

The information about the oligomer shape obtained from the extent of charging is analogous to that obtained from ion mobility measurements albeit at much lower resolution. However, CDMS has the advantage that it can be applied to much larger proteins making it possible to obtain information about size and shape in a size range (100's of MDa – GDa) that is difficult to measure using more conventional biophysical methods. Characterizing oligomers involved in the earliest stages of aggregation for full length Tau (~45 kDa), TDP-43 (~43 kDa), or even Huntington protein (~350 kDa) would provide insight into the molecular mechanisms of aggregation involved in neurological disease. Aggregation inhibition assays often require long periods of time (~hrs – days) to assay the formation of light-scattering particles under different solution conditions. CDMS measurements could accelerate these workflows by assaying the earliest stages of the aggregation process, providing quick feedback on the stabilizing effect of solution conditions or inhibitors that may significantly aid the development of

formulation/storage buffers for biopharmaceuticals or the discovery of novel compounds for inhibiting the aggregation of disease-causing amyloid-forming proteins.

Supporting Information. QTOF mass spectrum of 5 mg/mL BSA sample; Extended 1D mass histogram of heat-stressed 5 mg/mL BSA; QTOF mass spectrum of BSA from a denaturing solution; 2D mass-charge histogram of 5 mg/mL BSA; *m/z* mass spectrum of the data shown in Figure 2a; 2D mass-charge histogram of 0.1 mg/mL BSA before and after heat stress; Microscope images of BSA samples before and after heat stress; OD_{600} of heat-stressed BSA solutions; 2D mass-charge histogram of 25 mg/mL BSA after heat stress; 2D mass-charge histogram of 5 mg/mL BSA without and with heparin.

Acknowledgements

This work was supported by the National Science Foundation Division of Chemistry (grant number CHE-2203907), the National Institutes of Health (grant number 5R01GM139338) for development and construction of the CDMS instrument and data analysis methods used in this work, an ACS Graduate Research Fellowship sponsored by Eli Lilly and Company (JSJ), the Arnold and Mabel Beckman Foundation Postdoctoral Fellowship in Chemical Instrumentation (CCH), and Merck & Co., Inc., San Francisco, CA, USA, through their Discovery Biologics SEEDS program. The authors would like to thank Darren Kahan for assistance with OD_{600} measurements.

Author Contributions

All experiments were performed by JSJ. All coauthors contributed to the experimental design, data analysis, and writing of the manuscript. ERW directed the investigations.

Competing Interests

The authors declare no competing interests.

References

(1) Ross, C. A.; Poirier, M. A. Protein Aggregation and Neurodegenerative Disease. *Nat. Med.* **2004**, *10* (S7), S10–S17.

(2) Ratanji, K. D.; Derrick, J. P.; Dearman, R. J.; Kimber, I. Immunogenicity of Therapeutic Proteins: Influence of Aggregation. *J. Immunotoxicol.* **2014**, *11* (2), 99–109.

(3) Fekete, S.; Beck, A.; Veuthey, J. L.; Guillarme, D. Theory and Practice of Size Exclusion Chromatography for the Analysis of Protein Aggregates. *J. Pharm. Biomed. Anal.* **2014**, *101*, 161–173.

(4) Ray, S.; Mason, T. O.; Boyens-Thiele, L.; Farzadfard, A.; Larsen, J. A.; Norrild, R. K.; Jahnke, N.; Buell, A. K. Mass Photometric Detection and Quantification of Nanoscale α-Synuclein Phase Separation. *Nat. Chem.* **2023**, *15* (9), 1306–1316.

(5) Wu, D.; Piszczek, G. Measuring the Affinity of Protein-Protein Interactions on a Single-Molecule Level by Mass Photometry. *Anal. Biochem.* **2020**, *592* (November 2019), 113575.

(6) Hundt, N.; Cole, D.; Hantke, M. F.; Miller, J. J.; Struwe, W. B.; Kukura, P. Direct Observation of the Molecular Mechanism Underlying Protein Polymerization. *Sci. Adv.* **2022**, *8* (35), eabm7935.

(7) Liebthal, M.; Kushwah, M. S.; Kukura, P.; Dietz, K. J. Single Molecule Mass Photometry Reveals the Dynamic Oligomerization of Human and Plant Peroxiredoxins. *iScience* **2021**, *24* (11), 103258.

(8) Paul, S. S.; Lyons, A.; Kirchner, R.; Woodside, M. T. Quantifying Oligomer Populations in Real Time during Protein Aggregation Using Single-Molecule Mass Photometry. *ACS Nano* **2022**, *16* (10), 16462–16470.

(9) Pukala, T. L. Mass Spectrometric Insights into Protein Aggregation. *Essays Biochem.* **2023**, *67* (2), 243–253.

(10) Mehalebi, S.; Nicolai, T.; Durand, D. Light Scattering Study of Heat-Denatured Globular Protein Aggregates. *Int. J. Biol. Macromol.* **2008**, *43* (2), 129–135.

(11) Kundel, F.; Tosatto, L.; Whiten, D. R.; Wirthensohn, D. C.; Horrocks, M. H.; Klenerman, D. Shedding Light on Aberrant Interactions – a Review of Modern Tools for Studying Protein Aggregates. *FEBS J.* **2018**, *285* (19), 3604–3630.

(12) Bernstein, S. L.; Wyttenbach, T.; Baumketner, A.; Shea, J. E.; Bitan, G.; Teplow, D. B.; Bowers, M. T. Amyloid β-Protein: Monomer Structure and Early Aggregation States of Aβ42 and Its Pro^{19} Alloform. *J. Am. Chem. Soc.* **2005**, *127* (7), 2075–2084.

(13) Bernstein, S. L.; Dupuis, N. F.; Lazo, N. D.; Wyttenbach, T.; Condron, M. M.; Bitan, G.; Teplow, D. B.; Shea, J. E.; Ruotolo, B. T.; Robinson, C. V.; Bowers, M. T. Amyloid-β Protein Oligomerization and the Importance of Tetramers and Dodecamers in the Aetiology of Alzheimer's Disease. *Nat. Chem.* **2009**, *1* (4), 326–331.
(14) Bleiholder, C.; Dupuis, N. F.; Wyttenbach, T.; Bowers, M. T. Ion Mobility–Mass Spectrometry Reveals a Conformational Conversion from Random Assembly to β-Sheet in Amyloid Fibril Formation. *Nat. Chem.* **2011**, *3* (2), 172–177.
(15) Österlund, N.; Moons, R.; Ilag, L. L.; Sobott, F.; Graslund, A. Native Ion Mobility-Mass Spectrometry Reveals the Formation of β-barrel Shaped Amyloid-β Hexamers in a Membrane-Mimicking Environment. *J. Am. Chem. Soc.* **2019**, *141* (26), 10440–10450.
(16) Shahpasand-Kroner, H.; Portillo, J.; Lantz, C.; Seidler, P. M.; Sarafian, N.; Loo, J. A.; Bitan, G. Three-repeat and Four-repeat Tau Isoforms Form Different Oligomers. *Prot. Sci.* **2022**, *31* (3), 613–627.
(17) Stroganova, I.; Willenberg, H.; Tente, T.; Depraz Depland, A.; Bakels, S.; Rijs, A. M. Exploring the Aggregation Propensity of PHF6 Peptide Segments of the Tau Protein Using Ion Mobility Mass Spectrometry Techniques. *Anal. Chem.* **2024**, *96* (13), 5115–5124.
(18) Stroganova, I.; Toprakcioglu, Z.; Willenberg, H.; Knowles, T. P. J.; Rijs, A. M. Unravelling the Structure and Dynamics of Ac-PHF6-NH 2 Tau Segment Oligomers. *ACS Chem. Neurosci.* **2024**, *15* (18), 3391-3400.
(19) Depraz Depland, A.; Stroganova, I.; Wootton, C. A.; Rijs, A. M. Developments in Trapped Ion Mobility Mass Spectrometry to Probe the Early Stages of Peptide Aggregation. *J. Am. Soc. Mass Spectrom.* **2023**, *34* (2), 193–204.
(20) Laos, V.; Do, T. D.; Bishop, D.; Jin, Y.; Marsh, N. M.; Quon, B.; Fetters, M.; Cantrell, K. L.; Buratto, S. K.; Bowers, M. T. Characterizing TDP-$43_{307–319}$ Oligomeric Assembly: Mechanistic and Structural Implications Involved in the Etiology of Amyotrophic Lateral Sclerosis. *ACS Chem. Neurosci.* **2019**, *10* (9), 4112–4123.
(21) Frimpong, A. K.; Abzalimov, R. R.; Uversky, V. N.; Kaltashov, I. A. Characterization of Intrinsically Disordered Proteins with Electrospray Ionization Mass Spectrometry: Conformational Heterogeneity of α-synuclein. *Proteins* **2010**, *78* (3), 714–722.
(22) Moons, R.; Konijnenberg, A.; Mensch, C.; Van Elzen, R.; Johannessen, C.; Maudsley, S.; Lambeir, A. M.; Sobott, F. Metal Ions Shape α-Synuclein. *Sci. Rep.* **2020**, *10* (1), 16293.
(23) Phillips, A. S.; Gomes, A. F.; Kalapothakis, J. M. D.; Gillam, J. E.; Gasparavicius, J.; Gozzo, F. C.; Kunath, T.; MacPhee, C.; Barran, P. E. Conformational Dynamics of α-Synuclein: Insights from Mass Spectrometry. *Analyst* **2015**, *140* (9), 3070–3081.
(24) Hoffmann, W.; Folmert, K.; Moschner, J.; Huang, X.; von Berlepsch, H.; Koksch, B.; Bowers, M. T.; von Helden, G.; Pagel, K. NFGAIL Amyloid Oligomers: The Onset of Beta-Sheet Formation and the Mechanism for Fibril Formation. *J. Am. Chem. Soc.* **2018**, *140* (1), 244–249.
(25) Seo, J.; Hoffmann, W.; Warnke, S.; Huang, X.; Gewinner, S.; Schöllkopf, W.; Bowers, M. T.; von Helden, G.; Pagel, K. An Infrared Spectroscopy Approach to Follow β-Sheet Formation in Peptide Amyloid Assemblies. *Nat. Chem.* **2017**, *9* (1), 39–44.
(26) Bakels, S.; Daly, S.; Doğan, B.; Baerenfaenger, M.; Commandeur, J.; Rijs, A. M. Probing High-Order Transient Oligomers Using Ion Mobility Mass Spectrometry Coupled to Infrared Action Spectroscopy. *Anal. Chem.* **2024**, *96* (34), 13962-13970.

(27) Chowdhury, S. K.; Katta, V.; Chait, B. T. Probing Conformational Changes in Proteins by Mass Spectrometry. *J. Am. Chem. Soc.* **1990**, *112* (24), 9012–9013.
(28) Bush, M. F.; Hall, Z.; Giles, K.; Hoyes, J.; Robinson, C. V.; Ruotolo, B. T. Collision Cross Sections of Proteins and Their Complexes: A Calibration Framework and Database for Gas-Phase Structural Biology. *Anal. Chem.* **2010**, *82* (22), 9557–9565.
(29) Bischoff, A. J.; Harper, C. C.; Williams, E. R.; Francis, M. B. Characterizing Heterogeneous Mixtures of Assembled States of the Tobacco Mosaic Virus Using Charge Detection Mass Spectrometry. *J. Am. Chem. Soc.* **2022**, *144* (51), 23368–23378.
(30) Harper, C. C.; Elliott, A. G.; Oltrogge, L. M.; Savage, D. F.; Williams, E. R. Multiplexed Charge Detection Mass Spectrometry for High-Throughput Single Ion Analysis of Large Molecules. *Anal. Chem.* **2019**, *91* (11), 7458–7465.
(31) McGee, J. P.; Melani, R. D.; Yip, P. F.; Senko, M. W.; Compton, P. D.; Kafader, J. O.; Kelleher, N. L. Isotopic Resolution of Protein Complexes up to 466 kDa Using Individual Ion Mass Spectrometry. *Anal. Chem.* **2021**, *93* (5), 2723–2727.
(32) Du, C.; Cleary, S, P.; Kostelic;, M. M.; Jones;, B. J.; Kafader;, J. O.; Wysocki, V. H. Combining Surface-Induced Dissociation and Charge Detection Mass Spectrometry to Reveal the Native Topology of Heterogeneous Protein Complexes. **2023**, *95* (37), 13889-13896.
(33) Anthony, A. J.; Gautam, A. K. S.; Miller, L. M.; Ma, Y.; Hardwick, A. G.; Sharma, A.; Ghatak, S.; Matouschek, A.; Jarrold, M. F.; Clemmer, D. E. CDMS Analysis of Intact 19S, 20S, 26S, and 30S Proteasomes: Evidence for Higher-Order 20S Assemblies at a Low pH. *Anal. Chem.* **2023**, *95* (33), 12209–12215.
(34) Lai, S. H.; Tamara, S.; Heck, A. J. R. Single-Particle Mass Analysis of Intact Ribosomes by Mass Photometry and Orbitrap-Based Charge Detection Mass Spectrometry. *iScience* **2021**, *24* (11), 103211.
(35) Harper, C. C.; Miller, Z. M.; Lee, H.; Bischoff, A. J.; Francis, M. B.; Schaffer, D. V.; Williams, E. R. Effects of Molecular Size on Resolution in Charge Detection Mass Spectrometry. *Anal. Chem.* **2022**, *94* (33), 11703–11712.
(36) Barnes, L. F.; Draper, B. E.; Jarrold, M. F. Analysis of Recombinant Adenovirus Vectors by Ion Trap Charge Detection Mass Spectrometry: Accurate Molecular Weight Measurements beyond 150 MDa. *Anal. Chem.* **2022**, *94* (3), 1543–1551.
(37) Kostelic, M. M.; Ryan, J. P.; Brown, L. S.; Jackson, T. W.; Hsieh, C.; Zak, C. K.; Sanders, H. M.; Liu, Y.; Chen, V. S.; Byrne, M.; Aspinwall, C. A.; Baker, E. S.; Marty, M. T. Stability and Dissociation of Adeno-Associated Viral Capsids by Variable Temperature-Charge Detection-Mass Spectrometry. *Anal. Chem.* **2022**, *94* (34), 11723–11727.
(38) Pierson, E. E.; Keifer, D. Z.; Selzer, L.; Lee, L. S.; Contino, N. C.; Wang, J. C. Y.; Zlotnick, A.; Jarrold, M. F. Detection of Late Intermediates in Virus Capsid Assembly by Charge Detection Mass Spectrometry. *J. Am. Chem. Soc.* **2014**, *136* (9), 3536–3541.
(39) Tamara, S.; den Boer, M. A.; Heck, A. J. R. High-Resolution Native Mass Spectrometry. *Chem. Rev.* **2022**, *122* (8), 7269–7326.
(40) Miller, L. M.; Bond, K. M.; Draper, B. E.; Jarrold, M. F. Characterization of Classical Vaccines by Charge Detection Mass Spectrometry. *Anal. Chem.* **2021**, *93* (35), 11965–11972.
(41) McPartlan, M. S.; Harper, C. C.; Hanozin, E.; Williams, E. R. Ion Emission from 1–10 MDa Salt Clusters: Individual Charge State Resolution with Charge Detection Mass Spectrometry. *Analyst* **2024**, *149* (3), 735–744.

(42) Doussineau, T.; Bao, C. Y.; Antoine, R.; Dugourd, P.; Zhang, W.; D'Agosto, F.; Charleux, B. Direct Molar Mass Determination of Self-Assembled Amphiphilic Block Copolymer Nanoobjects Using Electrospray-Charge Detection Mass Spectrometry. *ACS Macro Lett.* **2012**, *1* (3), 414–417.
(43) Doussineau, T.; Désert, A.; Lambert, O.; Taveau, J. C.; Lansalot, M.; Dugourd, P.; Bourgeat-Lami, E.; Ravaine, S.; Duguet, E.; Antoine, R. Charge Detection Mass Spectrometry for the Characterization of Mass and Surface Area of Composite Nanoparticles. *J. Phys. Chem. C* **2015**, *119* (20), 10844–10849.
(44) Hanozin, E.; Harper, C. C.; McPartlan, M. S.; Williams, E. R. Dynamics of Rayleigh Fission Processes in ∼100 nm Charged Aqueous Nanodrops. *ACS Cent. Sci.* **2023**, *9* (8), 1611–1622.
(45) Harper, C. C.; Brauer, D. D.; Francis, M. B.; Williams, E. R. Direct Observation of Ion Emission from Charged Aqueous Nanodrops: Effects on Gaseous Macromolecular Charging. *Chem. Sci.* **2021**, *12* (14), 5185–5195.
(46) Harper, C. C.; Jordan, J. S.; Papanu, S.; Williams, E. R. Characterization of Mass, Diameter, Density, and Surface Properties of Colloidal Nanoparticles Enabled by Charge Detection Mass Spectrometry. *ACS Nano* **2024**, *18* (27), 17806–17814.
(47) Harper, C. C.; Miller, Z. M.; McPartlan, M. S.; Jordan, J. S.; Pedder, R. E.; Williams, E. R. Accurate Sizing of Nanoparticles Using a High-Throughput Charge Detection Mass Spectrometer without Energy Selection. *ACS Nano* **2023**, *17* (8), 7765–7774.
(48) Jordan, J. S.; Harper, C. C.; Zhang, F.; Kofman, E.; Li, M.; Sathiyamoorthy, K.; Zaragoza, J. P.; Fayadat-Dilman, L.; Williams, E. R. Charge Detection Mass Spectrometry Reveals Conformational Heterogeneity in Megadalton-Sized Monoclonal Antibody Aggregates. *J. Am. Chem. Soc.* **2024**, *146* (33), 23297–23305.
(49) den Boer, M. A.; Lai, S. H.; Xue, X.; van Kampen, M. D.; Bleijlevens, B.; Heck, A. J. R. Comparative Analysis of Antibodies and Heavily Glycosylated Macromolecular Immune Complexes by Size-Exclusion Chromatography Multi-Angle Light Scattering, Native Charge Detection Mass Spectrometry, and Mass Photometry. *Anal. Chem.* **2022**, *94* (2), 892–900.
(50) Wörner, T. P.; Thurman, H. A.; Makarov, A. A.; Shvartsburg, A. A. Expanding Differential Ion Mobility Separations into the MegaDalton Range. *Anal. Chem.* **2024**, *96* (14), 5392-5398.
(51) Jordan, J. S.; Xia, Z.; Williams, E. R. Tips on Making Tiny Tips: Secrets to Submicron Nanoelectrospray Emitters. *J. Am. Soc. Mass Spectrom.* **2022**, *33* (3), 607–611.
(52) Miller, Z. M.; Harper, C. C.; Lee, H.; Bischoff, A. J.; Francis, M. B.; Schaffer, D. V.; Williams, E. R. Apodization Specific Fitting for Improved Resolution, Charge Measurement, and Data Analysis Speed in Charge Detection Mass Spectrometry. *J. Am. Soc. Mass Spectrom.* **2022**, *33* (11), 2129–2137.
(53) Harper, C. C.; Miller, Z. M.; Williams, E. R. Combined Multiharmonic Frequency Analysis for Improved Dynamic Energy Measurements and Accuracy in Charge Detection Mass Spectrometry. *Anal. Chem.* **2023**, *95* (45), 16659–16667.
(54) Jordan, J. S.; Lee, K. J.; Williams, E. R. Overcoming Aggregation with Laser Heated Nanoelectrospray Mass Spectrometry: Thermal Stability and Pathways for Loss of Bicarbonate from Carbonic Anhydrase II. *Analyst* **2024**, *149* (8), 2281–2290.
(55) Susa, A. C.; Xia, Z.; Tang, H. Y. H.; Tainer, J. A.; Williams, E. R. Charging of Proteins in Native Mass Spectrometry. *J. Am. Soc. Mass Spectrom.* **2017**, *28* (2), 332–340.

(56) Yoshimura, Y.; Lin, Y.; Yagi, H.; Lee, Y. H.; Kitayama, H.; Sakurai, K.; So, M.; Ogi, H.; Naiki, H.; Goto, Y. Distinguishing Crystal-like Amyloid Fibrils and Glass-like Amorphous Aggregates from Their Kinetics of Formation. *Proc. Nat. Acad. Sci.* **2012**, *109* (36), 14446–14451.
(57) Ma, X. J.; Zhang, Y. J.; Zeng, C. M. Inhibition of Amyloid Aggregation of Bovine Serum Albumin by Sodium Dodecyl Sulfate at Submicellar Concentrations. *Biochem. (Mosc.)* **2018**, *83* (1), 60–68.
(58) Minsky, B. B.; Zheng, B.; Dubin, P. L. Inhibition of Antithrombin and Bovine Serum Albumin Native State Aggregation by Heparin. *Langmuir* **2014**, *30* (1), 278–287.
(59) Xu, Y.; Seeman, D.; Yan, Y.; Sun, L.; Post, J.; Dubin, P. L. Effect of Heparin on Protein Aggregation: Inhibition versus Promotion. *Biomacromolecules* **2012**, *13* (5), 1642–1651.
(60) Goedert, M.; Jakes, R.; Spillantini, M. G.; Hasegawa, M.; Smith, M. J.; Crowther, R. A. Assembly of Microtubule-Associated Protein Tau into Alzheimer-like Filaments Induced by Sulphated Glycosaminoglycans. *Nature* **1996**, *383* (6600), 550–553.
(61) Zhu, H.; Yu, J.; Kindy, M. S. Inhibition of Amyloidosis Using Low-Molecular-Weight Heparins. *Mol. Med.* **2001**, *7* (8), 517–522.
(62) Liu, X.; Zhang, W.; Liu, J.; Pearce, R.; Zhang, Y.; Zhang, K.; Ruan, Q.; Yu, Y.; Liu, B. Mg^{2+} Inhibits Heat-Induced Aggregation of BSA: The Mechanism and Its Binding Site. *Food Hydrocoll.* **2020**, *101* (2020), 105450.

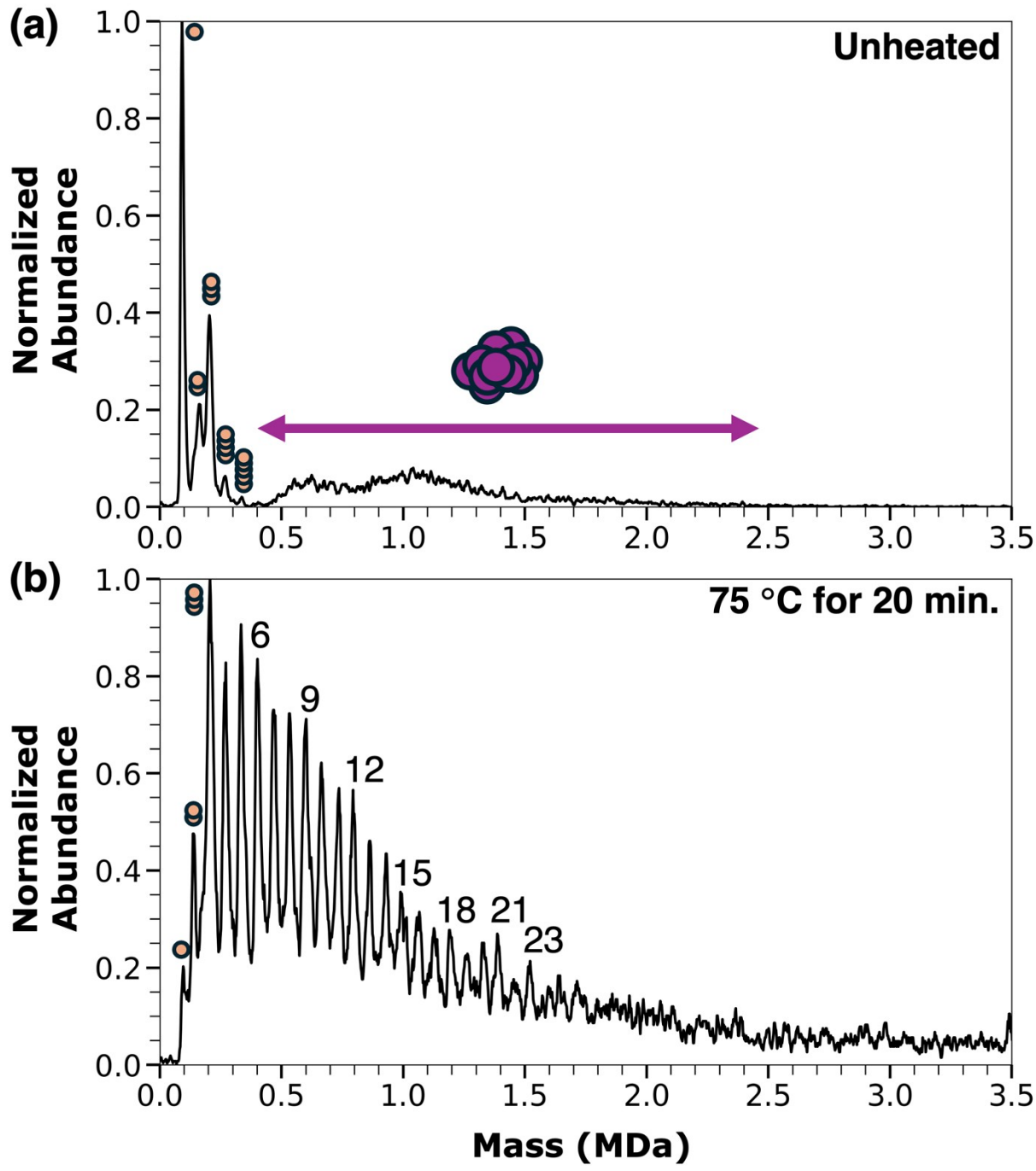

Figure 1. CDMS mass histograms of 5 mg/mL aqueous BSA solutions with 50 mM ammonium acetate (pH 6.8) (a) unheated and (b) heated at 75 ˚C for 20 min prior to cooling and filtering. The labels in (b) correspond to the number of BSA molecules in each oligomer.

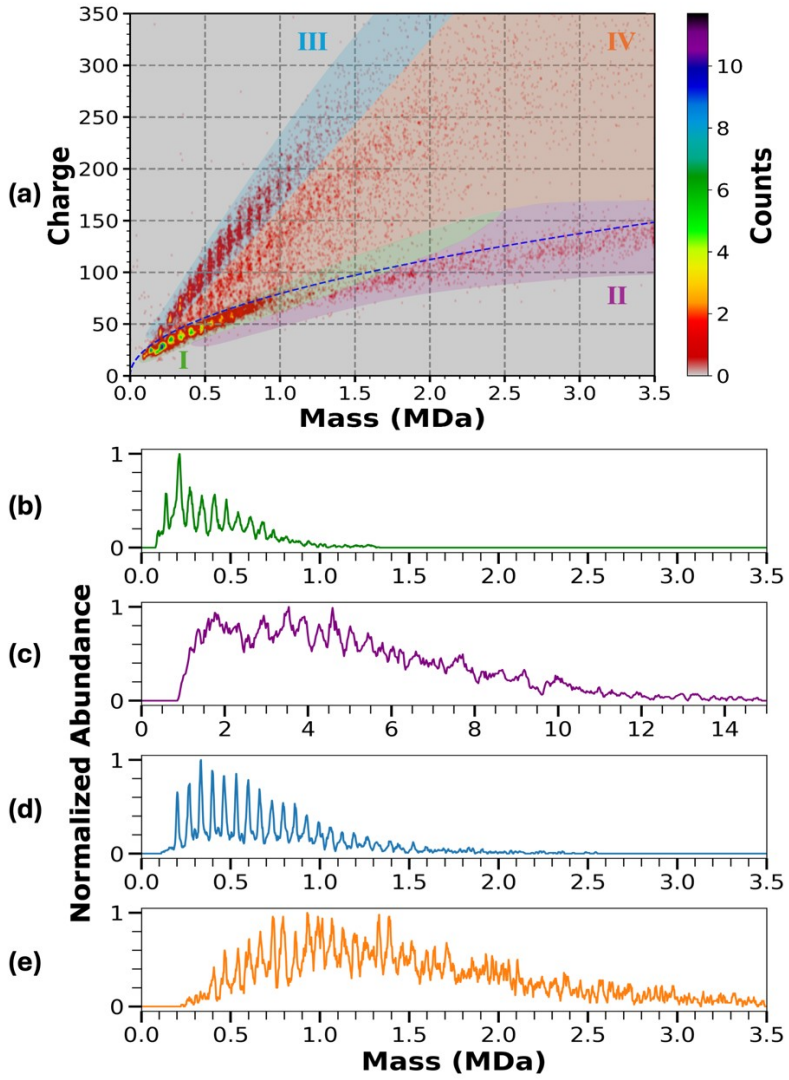

Figure 2. (a) 2-dimensional CDMS mass-charge data obtained from a 5 mg/mL aqueous solution of BSA (with 50 mM ammonium acetate, pH 6.8) heat stressed at 75 ˚C for 20 min. By selecting the individual families of conformers distinguished by the extent of oligomer charging, 1D mass histograms were extracted to show the different distributions of aggregate size for the (b) compact conformer family I (green), (c) higher mass and density conformer family II (purple), (d) elongated conformer family III (blue), and (d) partially elongated conformer family IV (orange). The blue dashed line represents the Rayleigh limit of an aqueous droplet as a function of mass.

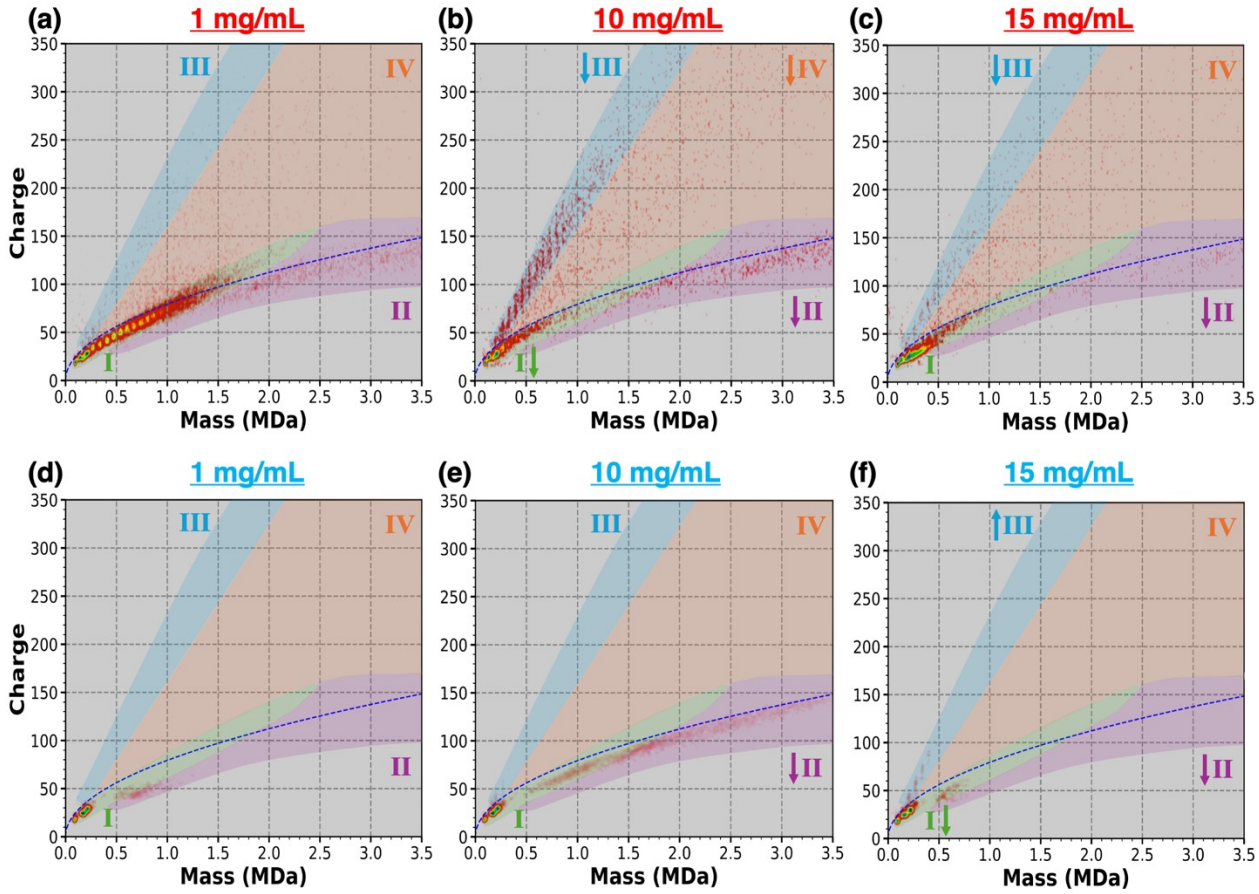

Figure 3. 2D mass-charge data obtained from aqueous BSA solutions (with 50 mM ammonium acetate, pH 6.8) at an initial BSA concentration of (a,d) 1 mg/mL, (b,e) 10 mg/mL, and (c,f) 15 mg/mL after heating at 75 ˚C for 20 min (a,b,c) and before heating (d,e,f). Shaded regions correspond to the same conformational families identified in Figure 2a. Arrows depict the increase or decrease in both abundance and size distribution for each conformational family relative to the lower concentrations. The arrows for the 10 mg/mL data depict the change in abundance and size distribution of each family relative to the 5 mg/mL data in Figures 2a and S3.

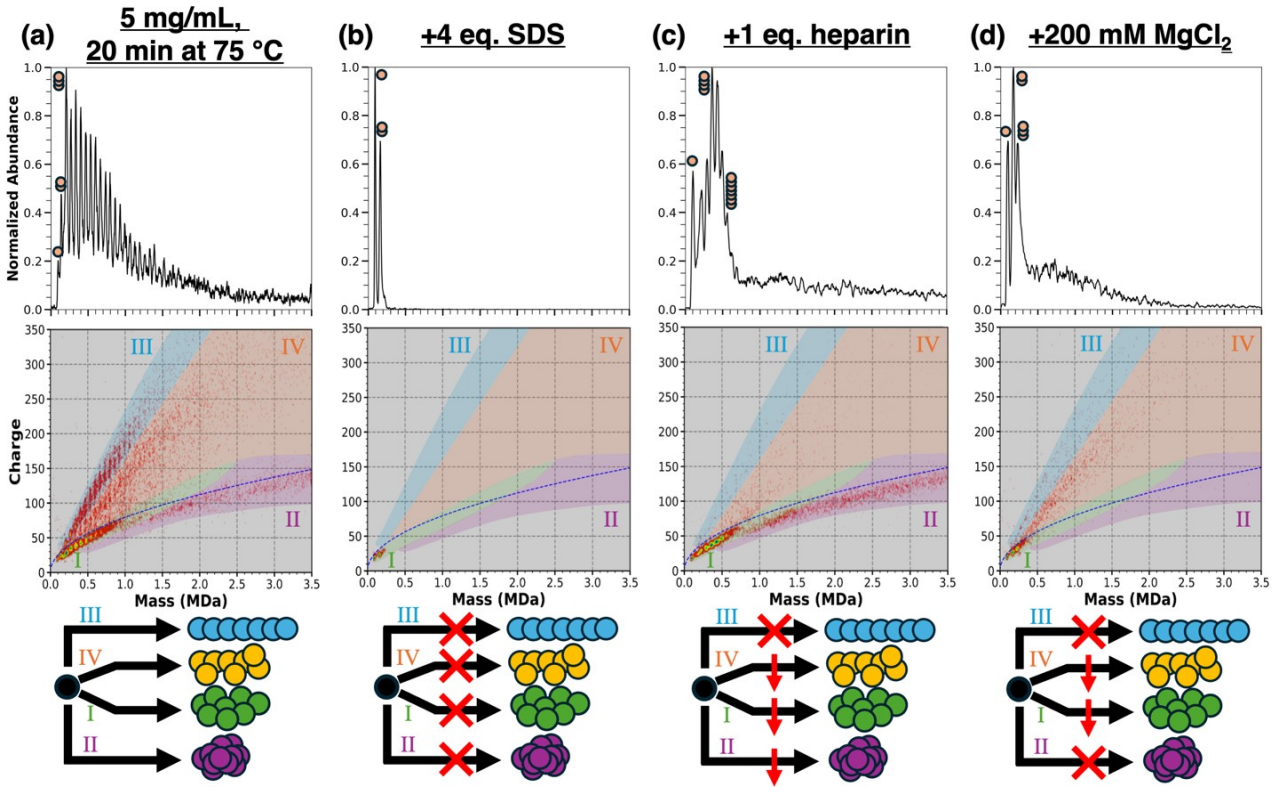

Figure 4. Mass histograms (top row) and 2D mass-charge data (middle row) of heat-stressed (75 °C for 20 min) BSA solutions (5 mg/mL BSA with 50 mM ammonium acetate, pH 6.8) containing (a) no inhibitor, (b) 4 molar eq. SDS, (c) 1 molar eq. heparin, or (d) 200 mM $MgCl_2$. The schemes in the bottom row indicate how each inhibitor affects the formation pathway for the four different conformational families. Shaded regions correspond to the same conformational families identified in Figure 2a.

For Table of Contents